Helmholtz-Zentrum Dresden-Rossendorf (HZDR)

HELMHOLTZ ZENTRUM
DRESDEN ROSSENDORF

Direct observation of the attachment behavior of hydrophobic colloidal particles onto a bubble surface

Nozomi, A.; Watanabe, S.; Miyahara, M. T.; Yamamoto, R.; Hampel, U.; Lecrivain, G.;

Originally published:

December 2019

Soft Matter 16(2020), 695

DOI: https://doi.org/10.1039/C9SM01787A

Perma-Link to Publication Repository of HZDR:

https://www.hzdr.de/publications/Publ-29611

Release of the secondary publication
on the basis of the German Copyright Law § 38 Section 4.

Soft Matter

Direct observation of the attachment behavior of hydrophobic colloidal particles onto a bubble surface

Journal:	*Soft Matter*
Manuscript ID	Draft
Article Type:	Paper
Date Submitted by the Author:	n/a

Complete List of Authors:	Arai, Nozomi; Kyoto University, Chemical Engineering Watanabe, Satoshi; Kyoto University, Chemical Engineering Miyahara, Minoru; Kyoto University, Chemical Engineering Yamamoto, Ryoichi; Kyoto University, Department of Chemical Engineering Hampel, Uwe; Helmholtz-Zentrum Dresden-Rossendorf, Institute fur Fluiddynamik; Technische Universitat Dresden, Institut fur Energietechnik Lecrivain, Gregory; Helmholtz Zentrum Dresden Rossendorf

Note: The following files were submitted by the author for peer review, but cannot be converted to PDF. You must view these files (e.g. movies) online.

S1.avi
S2.avi
S3.avi
S4.avi
S5.avi
S6.avi

SCHOLARONE™
Manuscripts

Direct observation of the attachment behavior of hydrophobic colloidal particles onto a bubble surface

Nozomi Arai[1], Satoshi Watanabe[1,*], Minoru T. Miyahara[1], Ryoichi Yamamoto[1], Uwe Hampel[2,3], and Gregory Lecrivain[2,]**

[1] Kyoto University, Department of Chemical Engineering, Katsura, Nishikyo, Kyoto 615-8510, Japan

[2] Helmholtz-Zentrum Dresden-Rossendorf, Institut für Fluiddynamik, Bautzner Landstraße 400, Dresden 01328, Germany

[3] Technische Universität Dresden, Institut für Energietechnik, Professur für Bildgebende Messverfahren für die Energie- und Verfahrenstechnik, Germany

*** nabe@cheme.kyoto-u.ac.jp**

**** g.lecrivain@hzdr.de**

Abstract

The attachment of solid particles to the surface of immersed gas bubbles plays a fundamental role in surface science, and hence plays key roles in various engineering fields ranging from industrial separation processes to the fabrication of functional materials. However, detailed investigation from a microscopic view on how a single particle attaches to a bubble surface and how the particle properties affect the attachment behavior has been so far scarcely addressed. Here, we observed the attachment of a single particle to a bubble surface using a high-speed camera and systematically investigated the effects of the wettability and shape of particles. We found that hydrophobic particles abruptly "jumped into" the bubble while sliding down the bubble surface to eventually satisfy their static contact angles, the behavior of which induced a much stronger attachment to the bubble surface. Interestingly, the determinant factor for the attachment efficiency of spherical particles was not the wettability of the spherical particles but the location of the initial collision with the bubble surface. In contrast, the attachment efficiency of anisotropically-shaped particles was found to increase with the hydrophobicity caused by a larger contact area to the bubble surface. Last but not least, a simple formulation is suggested to recover the contact angle based on the jump-in.

1. Introduction

The attachment of colloidal particles to the surface of an immersed gas bubble is of fundamental importance in many industrial and non-industrial applications.[1] The attachment mechanism in a gas-liquid system is strongly affected by the affinity of the particle surface. The coating of a gas bubble by multiple particle attachments is known to decrease the "apparent" surface tension of the gas-liquid interface. Hence particles can be used as a stabilizer,[2–6] in which the degree of the stabilization is determined by the liquid-air surface tension and the wettability of the particles. The attachment of microparticles to gas bubbles is used favorably in a wide range of industrial processes, including mineral flotation,[7] de-inking,[8,9] and wastewater treatment.[10] In such processes, the particle wettability is used for a selective separation. The mechanism behind the attachment of particles to a fluidic interface is not limited to air-liquid systems but it is also applied to liquid-air systems and liquid-liquid systems due to the universal effects played by the surface tension.[11,12] It enables for instance the fabrication of a variety of functional materials such as capsules,[13,14] hollow structures,[15,16] and dry water.[17,18]

A number of works have already been conducted on the coating of fluidic interfaces by particles. Most studies aimed to investigate the effect of surface tension on the resultant gas-bubble agglomerate.[12,14] These previous efforts have already led a basic understanding of the attachment mechanism. Yet, the dynamics of the attachment process is still not fully

understood despite its key role played in selective separation processes.[9,10,19,20]

The continuous development of imaging techniques has enabled the observation of single colloidal particles attaching to a bubble surface. Some previous works directly observed the attachment of particles to a fixed bubble and analyzed its dynamic process by image data processing.[21–26] These previous investigations have shown that both a) the initial position, at which a particle collides with the bubble surface, and b) the time required for the liquid film between the particle and bubble to rupture, have a determining effect on the dynamics of the particle attachment.[21,25,26] They have also demonstrated that the trajectories and the velocity evolutions of microspheres can be predicted based on the equation of motion including hydrodynamic forces.[22,26] The effects of particle shape on the attachment have also been investigated by using not only spherical particles but also anisotropic ones with elongated and angular shapes.[25,26] These studies largely focused on the hydrodynamic and physical properties of the particles, such as hydrodynamic forces and particle shapes, while the effect of chemical properties of the particles, such as the wettability, remains to be elucidated. In fact, the particle wettability is an essential factor in the bubble-particle attachment processes.

In the present study, we systematically investigated the effect of particle wettability on the particle-bubble attachment behaviors by the use of glass microspheres and “real-life” polyhedral-shaped glass particles with different degree of wettability through the direct

observation with a high-speed digital microscope. We analyzed the attachment by processing the captured videos and revealed unique attachment behavior specific to hydrophobic particles.

2. Experimental section

2.1. Materials

Spherical glass beads with diameters ranging from 63 μm to 88 μm (SGMT No. 007) were purchased from Toshinriko Co., Ltd. (Japan). Polyhedral shaped glass particles with sharp edges (GP75A-P) were purchased from Potters-Ballotini Co., Ltd. (Japan). The longest axis of polyhedral particles ranged from 75 μm to 150 μm. The particle sizes were reported by the manufacturers. Figures 1a and 1b show optical micrographs of the spherical and polyhedral particles, respectively. Cyclohexane (≥ 99.0%), chlorotrimethylsilane (TMCS, ≥ 99%), and hexamethyldisilazane (HMDS, ≥ 99%) were purchased from Sigma-Aldrich Co. LLC. (USA) and were used without further purification. We used ultrapure water with a resistivity of 18 MΩ·cm obtained from a Direct-Q3 UV water purification system (Millipore Corp., USA).

2.2. Particle surface modification

The surface of the glass beads was modified with either of two different silane coupling agents, TMCS or HMDS, to change the their wettability, the procedure of which is as

follows.[25] 0.012 g of TMCS or 0.005 g of HMDS was put into 20 mL of cyclohexane, to which 3.5 g of glass beads was added, followed by moderately stirring overnight so that the glass beads remained suspended to proceed the reaction of the glass bead surface with silane coupling agents. Afterwards, the glass beads were repeatedly settled down and redispersed in 20 mL of fresh cyclohexane to remove the unreacted silane coupling agents. The particles were then allowed to dry for a few hours in a fume hood at room temperature to let the cyclohexane evaporate safely and subsequently at 80 °C in an incubator to finally remove the remaining cyclohexane. We confirmed that the addition of a larger amount of silane coupling agents did not change the wettability of the resultant glass beads, indicating a complete modification over the whole surface of the glass beads. Because it was difficult to directly measure the contact angle of the surface-modified glass beads, we instead employed the sessile drop technique.[27,28] In this method, the contact angles formed by 5 μL droplets at rest on a flat glass substrate was measured. Prior to measuring the contact angle, the substrate surface had been modified with TMCS or HMDS. As shown in Figure 2, the contact angle strongly depended on the surface treatment. The measured contact angle of the untreated glass was 10º, those of surface modified glasses with HMDS and TMCS were 48º and 71º, respectively (Table 1).

Surface treatment	**Contact angle (θ)**
Untreated glass	10°
Glass treated with HMDS	48º

Glass treated with TMCS	71º

Table 1: Contact angles varied with two different surface treatments.

2.3. Bubble attachment experiment

Figure 3 shows a schematic of the experimental setup. We grew an air bubble at the tip of a needle placed horizontally in a tank filled with water. We subsequently observed the motion of particles settling towards the bubble with a high-speed digital microscope (VW-9000, Keyence Corp., Japan) with a frame rate of 250 fps. We gently immersed a thin needle with particles on its surface into the water and let the particles settle due to the action of gravity through a plastic tube placed right above the bubble as a guide to direct them towards the bubble. The needle, used to grow the gas bubble, was a hydrophobic one with a ta-C diamond-like carbon coating (Diamond MS Syringe 0355321, SGE Analytical Science), which was attached to a 50 μL or 25 μL precision syringe (50R-GT-MS1, 25R-GT-MS1, SGE Analytical Science). The use of the hydrophobic needle enabled the bubble to be stably attached to top of the needle tip. We set the bubble size between 1.3 mm and 1.5 mm because larger bubbles were easily detached from the needle while smaller ones were observed to deform into a non-spherical shape. We used spherical glass beads (untreated, HMDS-modified, and TMCS-modified) and polyhedral beads (untreated and TMCS-modified) to investigate the effects of the wettability and particle shape on bubble attachment behaviors. The recorded movies were analyzed by means of the post-processing program Fiji to

measure particle diameters and trace particle trajectories.

3. Results and Discussions

3.1. Attachment of an untreated spherical glass bead

Figure 4a shows the typical attachment of an untreated spherical glass bead with the contact angle θ = 10º onto a bubble. A series of snapshots were clipped every 0.06 s (every 15-frame). The trajectory and the velocity magnitude evolution of the bead center of mass are shown in Figures 4b and 4c. Hereafter the star superscript * is used to denote a quantity made non-dimensional with the bubble diameter (d_b) and the particle terminal velocity (u_∞). In that respect, the normalized coordinates of the particle center of mass are given by $x^* = x/d_\mathrm{b}$, $y^* = y/d_\mathrm{b}$ and its instantaneous velocity by $u^* = u/u_\infty$ (See Figure 4a-c). As seen in Figure 4c, a glass bead settling with the terminal velocity $u^* = 1$ eventually slows down in the vicinity of the bubble surface at position $y^* \approx 0.6$, possibly due to the lubrication effect[29] upon landing on the bubble surface with a collision angle $\phi_\mathrm{C} = 12°$. The collision angle (ϕ_C) is defined by the circular arc between the vertical *y*-axis and the segment connecting the bubble center to the particle center of mass at the initial location of collision (Figure 4a). The colliding bead then slides down the bubble surface (Figure 4b). It accelerates because of a gradual increase in the tangential component of the gravity force, $mg\sin(\phi)$, up to the maximum velocity $u^* \approx 1$, near the bubble equator at position $y^* =$

0. The term m is here the bead mass, g is the gravitational acceleration, and $\phi(t)$ is the instantaneous angle between the vertical *y*-axis and the segment connecting the bubble center to the center of mass of the sliding particle, and t is the time. The bead then gradually slows down due to the decrease in the gravity tangential component to eventually stop at the bottom pole of the bubble.

Figure 5a shows the velocity evolution of three beads with different values of $\phi_C = 12°$, $40°$, and $56°$. The increase in the collision angle (ϕ_C) is generally associated with a decrease in the total velocity drop reached upon collision with the bubble surface. This would be because smaller lubrication forces act on beads with larger incident angles that have small normal vectors of velocity against the bubble surface. With larger collision angles, for example with $\phi_C = 66°$ in Figure 5b, beads initially attaching to and sliding down the bubble surface were observed to later detach from the surface, here at around $y^* = -0.4$. Figure 5c shows an "attachment" chart showing the locations of the collisions with the bubble surface and the subsequent particle outcomes (either a full attachment or a detachment). The blue locations indicate a full attachment, and the red ones indicate a later detachment. The majority of the beads colliding beyond an angular position $\phi_C > 45°$, 84% of the beads to be precise, detached from the bubble surface, possibly because the sliding time was shorter than the induction time. The induction time is the time needed for the contact to be fully completed. For smaller collision angles, particles were found to

almost always stay attached because they had enough time for the contact with the fluidic interface to occur on the $y^* > 0$ region. The collision angle (ϕ_C) is thus a key parameter in determining the attachment efficiency of beads.

3.2. Effects of wettability on attachment behavior

TMCS-modified spherical beads with a contact angle of θ = 71º showed a peculiar behavior during the attachment to the gas bubble. As seen from the velocity magnitude evolution in Figure 6a, the velocity increased to $u^* = 1.3$ in a sudden manner at position $y^* = 0.1$. A closer look at the image sequence (Figure 6b) demonstrated that, during the sliding down the bubble surface, the bead rapidly penetrated the air-water interface, thereby satisfying the static contact angle of the TMCS-modified bead (see Supporting Information, Movie S1, where the penetration occurred approximately at t = 8 s). This phenomenon is similar to the so-called "jump-in" behavior reported in previous experimental studies.[23,24] Even though not all beads underwent the jump-in, beads that had jumped into the bubble surface never detached later. This in-turn suggests that the jump-in results in a much stronger adhesion to the bubble surface. The HMDS-modified spherical beads (θ = 48º) also exhibited a jump-in, yet with a lower depth of the penetration into the bubble than that of TMCS-modified beads (θ = 71º). This is simply due to their lower contact angles (see Supporting Information, Movie S2, where the jump-in occurred approximately at t = 5 s).

The maximum velocity right after the jump-in equated $u^* = 1.1$ (See Figure S1 in the Supporting Information) turned out to be smaller than that of the TMCS-modified beads (u^* = 1.3). These results suggest that the maximum sliding velocity changes depending on the bead surface area exposed to the water phase. The increased sliding velocity can be explained by a decreased fluid resistance acting on the bead at the interface[30] as shown in the schematic in Figure 6c and detailed in the theoretical work by Dörr *et al*.[31] as well as a decrease in the buoyancy. A smaller bead surface area exposed to the water due to a larger depth of penetration inside the bubble (hence a larger contact angle θ) leads to "partial" fluid resistance and buoyancy force from the water. This in-turn results in a velocity larger than the terminal velocity (u_∞) determined by the "full" fluid resistance and buoyancy only from water in the far-bubble region. To verify this, we estimated with a simple model the terminal velocity of sliding spherical bead as a function of the contact angle (θ) at the air–water interface and the polar angle (ϕ) (see Supporting Information for the calculation details). By solving the following equation

$$u^*(\phi,\theta) = \sin\phi\left(1 + \frac{\sin 2\theta}{2\pi} - \frac{\theta}{\pi}\right)^{-\frac{1}{2}}\left(\frac{4S - (2 - \cos^3\theta + 3\cos\theta)}{4(S-1)}\right) \qquad (1)$$

we found that, at the equator ($\phi = 90°$), $u^* = 1.3$ for θ = 48º and $u^* = 1.1$ for θ = 66º. These two values agree fairly well with the measured contact angles of the surface-modified beads, thereby demonstrating the validity of our proposed model for the jump-in behavior.

Here, $S = \rho_{\mathrm{P}}/\rho_{\mathrm{Liq}}$ is the bead-to-liquid density ratio and θ [rad] the static contact angle of the bead. This in-turn could lead to a novel technique to determine the contact angle of particles, which is generally difficult to directly measure, through the measurement of the particle velocity right after the jump-in.

Figure 7 shows the attachment charts of the surface-modified beads with different contact angles. Similar to the case of the untreated glass beads shown in Figure 5c, we observed that most of the beads detached in the region associated with larger ϕ_{C}, and interestingly, the attachment efficiency shows almost no dependence on the bead wettability. This result is closely related to the occurrence of the jump-in. In fact, we observed that most of the particles with a large ϕ_{C} did not jump in and eventually detached from the surface, possibly because they did not experience the radial component force of the gravity large enough to penetrate the surface against an energy barrier required to deform the meniscus shape. In that sense, it would be reasonable to assume that jump-in occurs not only for surface-modified beads but also for untreated ones with smaller collision angles. Both the penetration depth of the untreated glass beads (θ = 10°) and the sudden increase in the sliding velocity however are too short to be detected. The jump-in would thus dominantly determine the attachment behavior.

The above results demonstrate that the hydrophobic nature of particles does not increase the attachment efficiency. However, this seems to contradict flotation experiments so far

reported,[19] in which hydrophobic particles result in a higher recovery. This can be accounted for in terms of the attachment strength as follows. In our relatively simple experimental tests, the bubble was in a stationary position. In reality, the rising bubble is immersed in a turbulent agitated liquid flow, which in-turn causes the bubble to vibrate during its ascension. In a simple experiment, we therefore intentionally vibrated the particle-bubble aggregates, which were obtained after multiple particles had slid down the lower bubble pole. The untreated beads detached much more easily than the surface-modified beads (See Supporting Information, Movie S3 for the untreated and Movie S4 for the surface-modified beads). The stronger adhesive resistance of the surface-modified beads against vibrations would be because the beads that jumped into the bubble were trapped by stronger adhesive capillary force.[32] Our results thus demonstrate that chances for beads to be strongly trapped at the air-water interface by the jump-in are controlled by the collision angles of beads against a bubble, while the bead wettability affects the strength in the attachment.

3.3. Effects of particle shape on attachment behavior

In this section, polyhedral beads with sharp edges shown in Figure 1b were used. Figure 8a shows a typical attachment of a single untreated polyhedral bead. The bead ($\theta = 10°$) was found to weakly attach to a bubble surface with its sharp edge pointing toward the bubble surface, so that the contact area became as small as possible. In contrast, a TMCS-modified

polyhedral bead (θ = 71°) strongly attached to the bubble surface with its flat lateral side directly in contact with the bubble surface so as to make the contact area larger (See Figure 8b). In addition, the TMCS-modified polyhedral beads frequently showed jump-in-like behaviors, in which parts of the particles were abruptly sucked into the bubble (see Supporting Information, Movie S5 and S6 for untreated and surface-modified polyhedral beads, where the jump-in-like behavior occurred approximately at t = 8 s in movie S6). This led to a dramatic difference in the attachment efficiency. Unlike the case of the spherical beads, we observed that most of the untreated polyhedral beads detached from the bubble surface regardless of the collision angles ϕ_C, while most of the TMCS-modified ones were able to stay attached. These results demonstrate that the effect of wettability is highly enhanced for polyhedral beads because of their anisotropic shape that enables the adhesion with their flat side.

4. Conclusions

We have directly observed the attachment behaviors of silica beads to a bubble surface with a high-speed digital microscope. Through our systematic investigation on the effects of the hydrophobicity and shape of beads, the following conclusions are drawn:

1) Hydrophobic beads exhibit the so-called jump-in behavior during sliding on a bubble surface, in which they abruptly penetrate the air-water interface so that their static contact

angles are eventually satisfied. The jump-in behavior strongly traps the beads at the air-water interface and keeps them against the intentional vibration of the bubble.

2) The jump-in behavior is characterized by a stepwise increase in the bead velocity which is caused by the decrease in the fluid resistance acting on a bead due to the replacement of a part of the surrounding fluid from water to air. Our simple calculation confirmed that the contact angle of a bead determines the terminal velocity after the jump-in. This in turn could enable the measurement of the contact angles of particles.

3) The collision angle dominantly determines the attachment efficiency of beads. Beads with small collision angles stay attached on the bubble surface, while those with large collision angles eventually detached. In the case of spherical beads, the hydrophobicity of beads has almost no effect on the attachment efficiency.

4) In the case of anisotropic-shaped beads, the effect of the bead hydrophobicity was highly enhanced, thereby inducing the difference in the attachment behavior unlike the case of the spherical beads. While untreated polyhedral beads attached to a bubble with a sharp edge pointing towards the surface, the hydrophobized ones attached with a lateral side facing a bubble surface to create a large contact area, which in-turn dramatically improved the attachment efficiency.

Conflicts of interest

There are no conflicts to declare.

Acknowledgements

This work was partially supported by a Marie Curie International Outgoing Fellowship with the European Union Seventh Framework Program for Research and Technological Development (2007-2013) under the grant agreement number 623518.

Electronic Supplementary Information

Electronic Supplementary Information (ESI) available: Videos of a glass bead showing jump-in behavior, strength of resistance against the vibration, and attachment behavior of polyhedral beads. See DOI: 10.1039/x0xx00000x

References

1 G. Lecrivain, Y. Kotani, R. Yamamoto, U. Hampel and T. Taniguchi, *Phys. Rev. Fluids*, 2018, **3**, 1.

2 W. Ramsden and FrancisGotch, *Proc. R. Soc. London*, 1904, **72**, 156.

3 S. Pickering, *J. Chem. Soc. Trans.*, 1907, 2001.

4 S. Fujii, A. J. Ryan and S. P. Armes, *J. Am. Chem. Soc.*, 2006, **128**, 7882.

5 S. Fujii, P. D. Iddon, A. J. Ryan and S. P. Armes, *Langmuir*, 2006, **22**, 7512.

6 Z. A. AlYousef, M. A. Almobarky and D. S. Schechter, *J. Colloid Interface Sci.*, 2018, **511**, 365.

7 A. Nguyen and H. J. Schulze, *Colloidal Science of Flotation*, CRC Press, 2003.

8 J. K. Borchardt, *Colloids Surfaces A Physicochem. Eng. Asp.*, 1994, **88**, 13.

9 B. Johansson, R. J. Pugh and L. Alexandrova, *Colloids Surfaces A Physicochem. Eng. Asp.*, 2000, **170**, 217.

10 J. Rubio, M. . Souza and R. . Smith, *Miner. Eng.*, 2002, **15**, 139.

11 B. P. Binks, *Curr. Opin. Colloid Interface Sci.*, 2002, **7**, 21.

12 R. Aveyard, B. P. Binks and J. H. Clint, *Adv. Colloid Interface Sci.*, 2003, **100**–**102**, 503.

13 A. D. Dinsmore, M. F. Hsu, M. G. Nikolaides, M. Marquez, A. R. Bausch and D. A. Weitz, *Science*, 2002, **298**, 1006.

14 S. Lam, K. P. Velikov and O. D. Velev, *Curr. Opin. Colloid Interface Sci.*, 2014, **19**, 490.

15 T. Chen, P. J. Colver and S. A. F. Bon, *Adv. Mater.*, 2007, **19**, 2286.

16 M. Li, Y. Zhang, X. Wang, W. Ahn, G. Jiang, K. Feng, G. Lui and Z. Chen, *Adv. Funct. Mater.*, 2016, **26**, 8408.

17 B. P. Binks and R. Murakami, *Nat. Mater.*, 2006, **5**, 865.

18 W. Wang, C. L. Bray, D. J. Adams and A. I. Cooper, *J. Am. Chem. Soc.*, 2008, **130**,

11608.

19 P. Blake and J. Ralston, *Colloids and Surfaces*, 1985, **16**, 41.

20 P. T. L. Koh, F. P. Hao, L. K. Smith, T. T. Chau and W. J. Bruckard, *Int. J. Miner. Process.*, 2009, **93**, 128.

21 W. Wang, Z. Zhou, K. Nandakumar, Z. Xu and J. H. Masliyah, *Int. J. Miner. Process.*, 2003, **68**, 47.

22 W. Wang, Z. Zhou, K. Nandakumar, Z. Xu and J. H. Masliyah, *J. Colloid Interface Sci.*, 2003, **259**, 81.

23 A. V. Nguyen and G. M. Evans, *Exp. Therm. Fluid Sci.*, 2004, **28**, 381.

24 D. I. Verrelli, P. T. L. Koh and A. V. Nguyen, *Chem. Eng. Sci.*, 2011, **66**, 5910.

25 D. I. Verrelli, W. J. Bruckard, P. T. L. Koh, M. P. Schwarz and B. Follink, *Miner. Eng.*, 2014, **58**, 80.

26 G. Lecrivain, G. Petrucci, M. Rudolph, U. Hampel and R. Yamamoto, *Int. J. Multiph. Flow*, 2015, **71**, 83.

27 T. Young, *Philos. Trans. R. Soc. London*, 1805, **95**, 65.

28 D. Y. Kwok and A. W. Neumann, *Adv. Colloid Interface Sci.*, 1999, **81**, 167.

29 B. Albijanic, O. Ozdemir, A. V. Nguyen and D. Bradshaw, *Adv. Colloid Interface Sci.*, 2010, **159**, 1.

30 J. T. Petkov, N. D. Denkov, K. D. Danov, O. D. Velev, R. Aust and F. Durst, *J.*

Colloid Interface Sci., 1995, **172**, 147.

31 A. Dörr, S. Hardt, H. Masoud and H. A. Stone, *J. Fluid Mech.*, 2016, **790**, 607.

32 A. V. Nguyen, *Int. J. Miner. Process.*, 2003, **68**, 167.

FIGURE CAPTIONS

Figure 1. Optical images of particles used in the experiments: (a) spherical glass beads and (b) polyhedral glass particles with sharp edges. Scale bars in (a) and (b) indicate 50 μm and 100 μm, respectively.

Figure 2. Contact angles of water on (a) untreated glass plate, (b) glass plate modified with HMDS, and (c) glass plate modified with TMCS. Measured angles are (a) 10º, (b) 48º, and (c) 71º.

Figure 3. Schematic illustration of the experimental setup.

Figure 4. Typical attachment behavior of an untreated glass bead with ϕ_C of 12º: (a) snapshots clipped at every 0.06 s, (b) trajectory of the bead, and (c) evolution of the bead velocity magnitude. A scale bar in (a) indicates 100 μm.

Figure 5. Differences in attachment behaviors for different ϕ_C values: (a) evolution of the particle velocity magnitude, (b) snapshots clipped at every 0.06 sec of an untreated bead

which becomes detached from a bubble, and (c) attachment chart where the green line indicates a bubble surface. In (c), red crosses are plotted with a wider margin from the bubble surface than that for blue circles so as to avoid overlap between crosses and circles for clarity. A scale bar in (b) indicates 100 μm.

Figure 6. Attachment behavior of a TMCS-modified glass bead with ϕ_C of 27º: (a) evolution of the bead velocity magnitude and (b) snapshots clipped at every 0.03 sec at the moment when a TMCS-modified particle jumps in the bubble surface. (c) Schematic of a glass bead right after jump-in where θ is a static contact angle of a bead. A scale bar in (b) indicates 100 μm.

Figure 7. Attachment charts of (a) HMDS-modified beads with the contact angle of 48º and (b) TMCS-modified beads with the contact angle of 71º. The green line indicates a bubble surface, and red crosses are plotted with a wider margin from the bubble surface than that for blue circles so as to avoid overlap between crosses and circles for clarity.

Figure 8. Snapshots clipped at every 0.03 sec of attachment motions of (a) an untreated polyhedral bead and (b) a TMCS-modified polyhedral one. All scale bars indicate 100 μm.

3 September 2019

Dear Editor:

I wish to submit an article for publication in the Soft Matter titled "**Direct observation of the attachment behavior of hydrophobic colloidal particles onto a bubble surface**". The paper has been coauthored by Nozomi Arai, Satoshi Watanabe, Minoru T. Miyahara, Ryoichi Yamamoto, Uwe Hampel, and Gregory Lecrivain.

We conducted the direct observation of a single particle attaching on a bubble with a high-speed camera and examined the effects of the wettability and shape of particles on the dynamics of the attachment behavior. Our findings reveal that the strong attachment on a bubble surface is induced by "jump-in" behavior, in which hydrophobic particles abruptly penetrate the air-water interface during sliding on the bubble surface to satisfy their static contact angles. We also confirmed that the attachment efficiency of spherical particles is not determined by the wettability of particles but the location of the initial collision on a bubble surface, while that of anisotropically-shaped particles increases with the hydrophobicity of particles because they are more stabilized by attaching with a flat side of a larger contact area facing to the bubble surface.

We believe that our study makes an important contribution to the fundamental science on soft matter because the particle attachment on a bubble is a fundamental phenomenon in surface science, and therefore, has a high applicability. This phenomenon can find applications in a wide range of fields from the separation process on an industrial scale to the fabrication of the functional materials. A lot of works have so far dealt with this fundamental phenomenon. Their main focus has been in structures, properties, and functionality of bubbles covered with particles, or separation efficiencies from a macroscopic point of view in floatation processes. However, detailed mechanism, especially dynamics of attachment behaviors, has not yet been clarified in spite of the importance in a number of engineering fields such as the separation process and the fabrication of functional materials. An attractive point of our work is analyzing the dynamic process of the attachment from a microscopic view, which provides fundamental understandings. Hence, we believe that the experimental technique and findings reported in our work will appeal to the scientists in the field of surface chemistry who subscribe to Soft Matter. We received "Soft Matter Award" at an international conference (IUMRS-ICAM 2017) from Royal Society of Chemistry, which also demonstrates the suitability of our manuscript to the journal, *Soft Matter*.
(http://blogs.rsc.org/sm/category/oral-presentation-prize/)

This manuscript contains a Supporting Information of additional explanation and a figure (PDF), and 6 movies (AVI).

This manuscript has not been published or presented elsewhere in part or in entirety and is not under consideration by another journal. We have read and understood your journal's policies, and we believe that neither the manuscript nor the study violates any of these. There are no conflicts of interest to declare.

Thank you for your consideration. I look forward to hearing from you.

Sincerely,
Satoshi Watanabe
Department of Chemical Engineering
Kyoto University
Katsura, Nishikyo, Kyoto 615-8510 Japan.
Phone: +81-75-383-2672

Fax: +81-75-383-2652
Email: nabe@cheme.kyoto-u.ac.jp

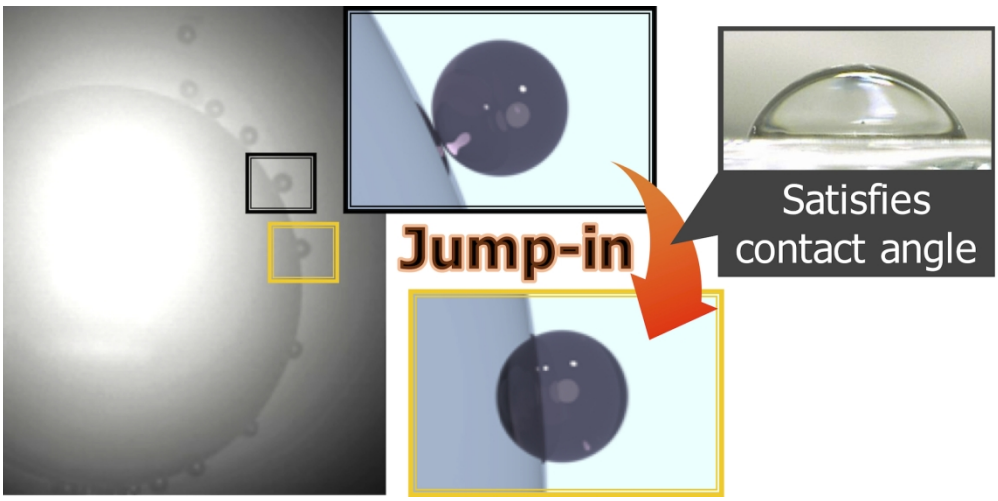

79x39mm (600 x 600 DPI)

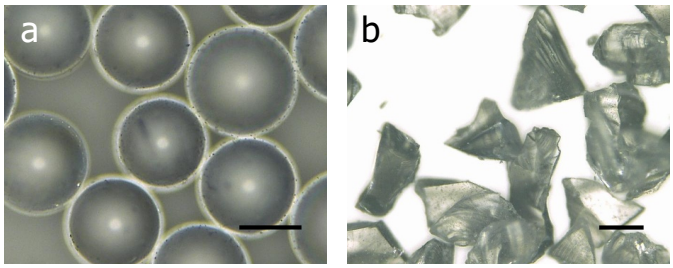

Figure 1

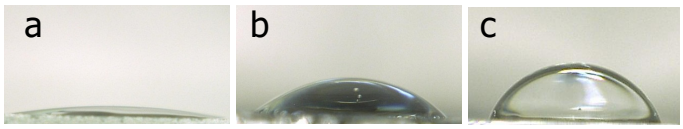

Figure 2

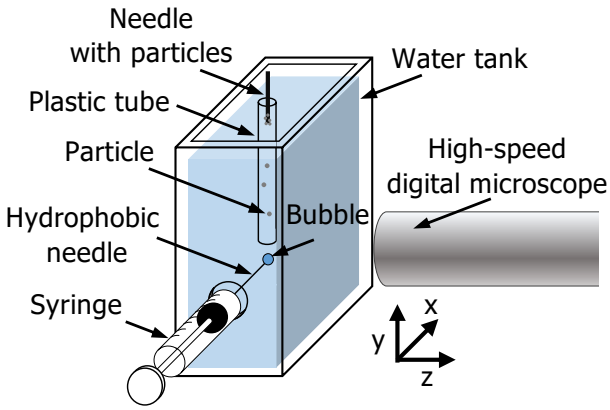
Needle
with particles
Water tank
Plastic tube
Particle
High-speed
digital microscope
Hydrophobic
needle
Bubble
Syringe
x
y
z

Figure 3

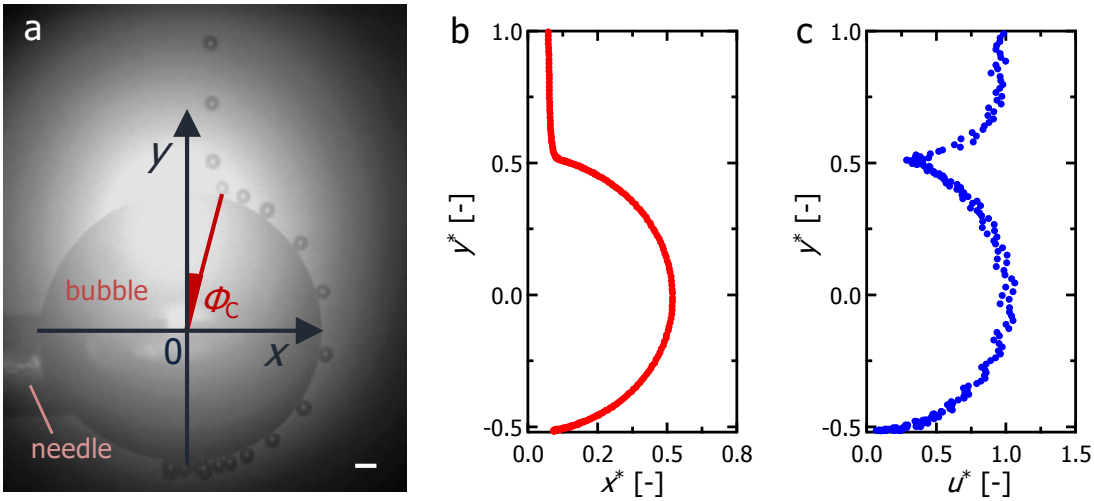
a
y
bubble
Φ_C
0
x
needle
b
1.0
0.5
0.0
-0.5
y^* [-]
0.0
0.2
0.5
0.8
x^* [-]
c
1.0
0.5
0.0
-0.5
y^* [-]
0.0
0.5
1.0
1.5
u^* [-]

Figure 4

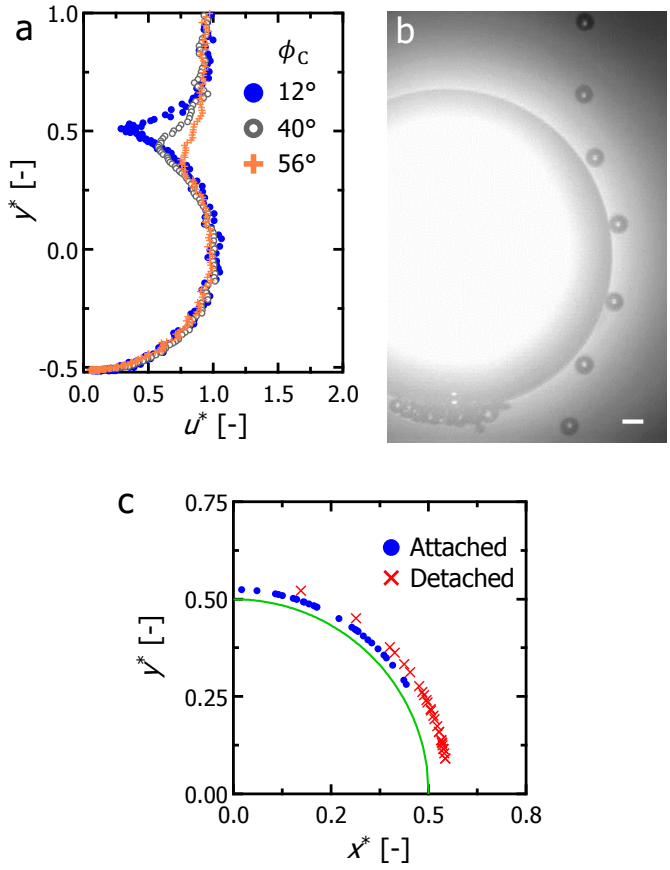

Figure 5

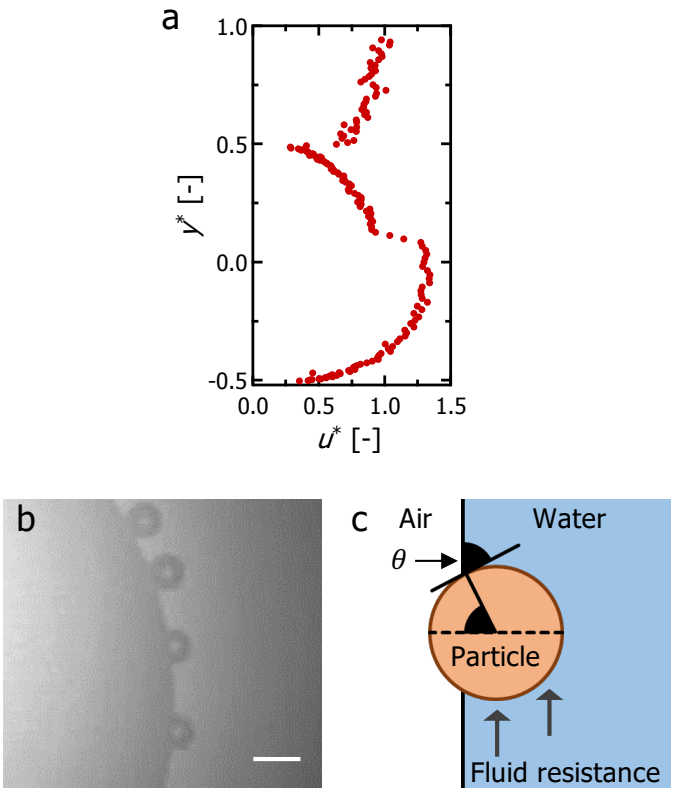
a
1.0
0.5
0.0
-0.5
y* [-]
0.0
0.5
1.0
1.5
u* [-]
b
c
Air
Water
θ
Particle
Fluid resistance

Figure 6

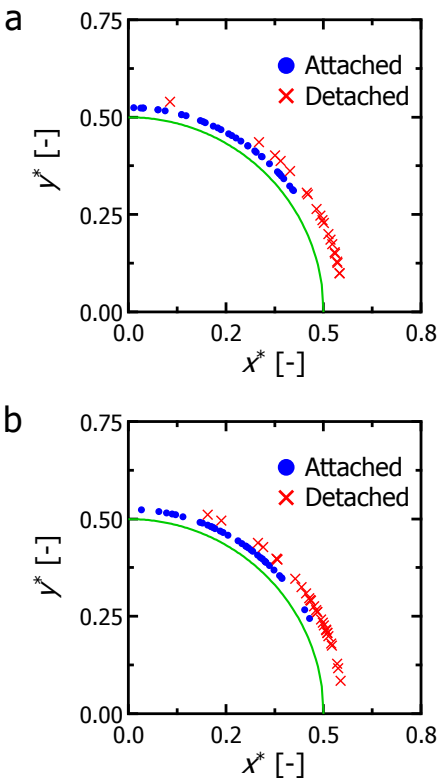

Figure 7

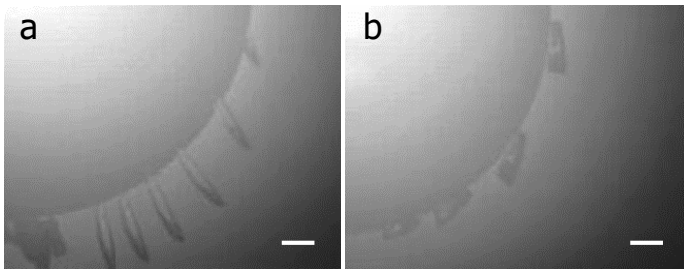

Figure 8

Supporting information for

Direct observation of the attachment behavior of hydrophobic colloidal particles onto a bubble surface

Nozomi Arai[1], Satoshi Watanabe[1,*], Minoru T. Miyahara[1], Ryoichi Yamamoto[1], Uwe Hampel[2,3], and Gregory Lecrivain[2,**]

[1] *Kyoto University, Department of Chemical Engineering, Katsura, Nishikyo, Kyoto 615-8510, Japan*

[2] *Helmholtz-Zentrum Dresden-Rossendorf, Institut für Fluiddynamik, Bautzner Landstraße 400, Dresden 01328, Germany*

[3] *Technische Universität Dresden, Institut für Energietechnik, Professur für Bildgebende Messverfahren für die Energie- und Verfahrenstechnik, Germany*

* nabe@cheme.kyoto-u.ac.jp

** g.lecrivain@hzdr.de

Velocity evolution in the case of a HMDS-modified bead

Figure S1 shows the velocity evolution of a HMDS-modified bead through an attachment event. The bead exhibited the jump-in behavior right after landing, and the maximum velocity was larger than u^* = 1.0. The increase in the velocity of HMDS-modified beads is smaller than that of TMCS-modified ones because the fluid resistance did not decrease largely owing to a small degree of the penetration into a bubble.

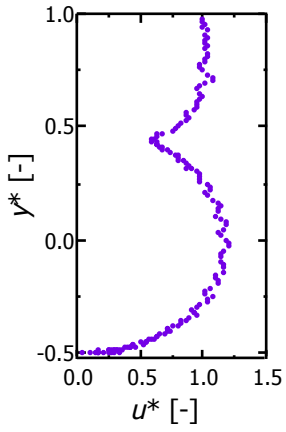

Figure S1. Velocity evolution of a HMDS-modified bead through an attachment event

Calculation procedure to obtain a static contact angle from a velocity of a particle

We assumed that the step-wise increase in a particle velocity was induced by the decrease in the fluid resistance due to the jump-in to satisfy the static contact angle of a particle surface (see Figure 6c). Based on this assumption, the static contact angle, θ [rad], was calculated from the maximum velocity, which is determined by the immersed part of the area of a particle in water. The projected area A_{pAir} [m^2] and volume V_{Air} [m^3] of the exposed potion of a single particle to the air are expressed as Equations (1) and (2). Those of the immersed portion of the particle in water, A_{pLiq} [m] and V_{Liq} [m^3], are given by subtracting A_{pAir} and V_{Air} from the whole surface area and volume as in Equations (3) and (4).

$$A_{\mathrm{pAir}} = \frac{d_{\mathrm{p}}^2}{2}\int_0^{\theta}(1-\cos^2\alpha)d\alpha = \frac{d_{\mathrm{p}}^2}{8}(2\theta - \sin 2\theta) \tag{1}$$

$$V_{\mathrm{Air}} = \frac{\pi d_{\mathrm{p}}^3}{8}\int_0^{\theta}(1-\cos^2\alpha)\sin\alpha\, d\alpha = \frac{\pi d_{\mathrm{p}}^3}{8}\left(\frac{2}{3}+\frac{1}{3}\cos^3\theta - \cos\theta\right) \tag{2}$$

$$A_{\mathrm{pLiq}} = \frac{\pi d_{\mathrm{p}}^2}{4} - A_{\mathrm{pAir}} \tag{3}$$

$$V_{\mathrm{Liq}} = \frac{\pi d_{\mathrm{p}}^3}{6} - V_{\mathrm{Air}} \tag{4}$$

Here, d_{p} [m] is the diameter of the particle, and α [rad] is the angle between a tangential line of a bead and air-water interface (see Fig 6c, where it is expressed as θ [rad]). Fluid resistance, F_{D} [N], is then expressed as a function of Re_{pAir} [−] and Re_{pLiq} [−], which are the Reynolds numbers in air and water respectively,[1,2] because both Reynolds numbers are smaller than 2, which is in the Stokes region.

$$F_D = \frac{1}{2}\frac{24}{Re_{\mathrm{pAir}}}A_{\mathrm{pAir}}\rho_{\mathrm{Air}}u^2 + \frac{1}{2}\frac{24}{Re_{\mathrm{pLiq}}}A_{\mathrm{pLiq}}\rho_{\mathrm{Liq}}u^2$$
$$= \frac{1}{2}\frac{24\mu_{\mathrm{Air}}}{\rho_{\mathrm{Air}}d_{\mathrm{pAir}}u}A_{\mathrm{pAir}}\rho_{\mathrm{Air}}u^2 + \frac{1}{2}\frac{24\mu_{\mathrm{Liq}}}{\rho_{\mathrm{Liq}}d_{\mathrm{pLiq}}u}A_{\mathrm{pLiq}}\rho_{\mathrm{Liq}}u^2 \quad (5)$$
$$= \frac{12\,\mu_{\mathrm{Air}}A_{\mathrm{pAir}}}{d_{\mathrm{pAir}}}u + \frac{12\,\mu_{\mathrm{Liq}}A_{\mathrm{pLiq}}}{d_{\mathrm{pLiq}}}u$$

$$d_{\mathrm{pAir}} = \sqrt{\frac{4A_{\mathrm{pAir}}}{\pi}} \quad (6)$$

$$d_{\mathrm{pLiq}} = \sqrt{\frac{4A_{\mathrm{pLiq}}}{\pi}} \quad (7)$$

Here, u [m/s] is the velocity of a bead. μ_{Air} [Pa · s] and μ_{Liq} [Pa · s] indicate the viscosity of air and water, respectively. ρ_{Air} [kg/m^3] and ρ_{Liq} [kg/m^3] are the density of air and liquid, respectively. The buoyancy force, F_{B} [N], is expressed by the following equation.

$$F_{\mathrm{B}} = \rho_{\mathrm{Air}}V_{\mathrm{Air}}g + \rho_{\mathrm{Liq}}V_{\mathrm{Liq}}g \quad (8)$$

In the events of the particle attachment, the inertia can be neglected due to small Reynolds numbers. The terminal velocity of the particle is determined by the balance between the fluid resistance and the external force acting on a particle as in Equation (9).

$$0 = \frac{\pi}{6}\rho_{\mathrm{p}}d_{\mathrm{p}}^3\mathrm{g}\sin\phi\ - F_{\mathrm{D}} - F_{\mathrm{B}}\sin\phi \quad (9)$$

Here, ρ_{P} [kg/m^3] is the density of a particle, and ϕ [rad] is the instantaneous angle between the vertical y-axis and the segment connecting the bubble center to the center of mass of the sliding particle. Because the viscosity and density of air are much smaller than those of water, the fluid resistance and buoyancy force of air can be neglected. Finally, we get the following formula.

$$u^*(\phi,\theta) = \sin\phi\left(1+\frac{\sin 2\theta}{2\pi}-\frac{\theta}{\pi}\right)^{-\frac{1}{2}}\left(\frac{4S-(2-\cos^3\theta+3\cos\theta)}{4(S-1)}\right) \quad (10)$$

Here, $S = \rho_{\mathrm{P}}/\rho_{\mathrm{Liq}}$ is the bead-to-liquid density ratio. Equation (10) gives the relationship between the velocity u and the static contact angle θ of a particle. Hence, the static contact angle can be uniquely determined from the maximum velocity of a particle after the jump-in.

References

1 G. G. Stokes, *Trans. Cambridge Philos. Soc.*, 1850, **IX**, 8.

2 A. Haider and O. . Levenspiel, *Powder Technol.*, 1989, **58**, 63.